Mediterranean Archaeology and Archaeometry, Vol. 11, No. 2, pp. 107-120

IRSL DATING OF A DEEP WATER CORE FROM PYLOS, GREECE; COMPARISON TO POST IR BLUE OSL AND TL DATING RESULTS

George S. Polymeris[a,b], George Kitis[c]

[a] *Laboratory of Radiation Applications and Archaeological Dating, Department of Archaeometry and Physicochemical Measurements, Cultural and Educational Technology Institute, 'Athena' - Research and Innovation Center in Information, Communication and Knowledge Technologies, Tsimiski 58, GR-67100, Xanthi, Greece*

[b] *IŞIK University, Faculty of Science and Arts, Physics Department, Şile 34980 – Istanbul, Turkey*

[c] *Physics Department, Aristotle University of Thessaloniki, GR – 54124 Thessaloniki, Greece*

Received: 23/02/2010
Accepted: 14/06/2011
Corresponding author: polymers@auth.gr

ABSTRACT

The 'double SAR' protocol procedure permits the determination of two equivalent dose (*De)* values for each polymineral aliquot; an IRSL *De* resulting mostly from feldspars along with a post-IR OSL *De* for a mixed signal for quartz (mostly) and feldspar grains. The objective of the present study is to test for the first time its usefulness for polymineral, coarse silt, closely-spaced deep-sea sediment samples. A new, 'double SAR' IRSL dataset is presented for the sedimentation ages of a deep-sea sediment core of the Hellenic Trench, drilled from a water depth of 4 km, near the deepest site of the Mediterranean Sea, outside Pylos, Greece. Post IR quartz-based optical dating was previously proved to be consistent with AMS radiocarbon ages, obtained from planktonic foraminifera from the same core. IRSL *De* values are, with one exception, always much greater than the corresponding (post-IR) OSL results. This result suggests that for the present study 'double SAR' protocol procedure was proved to be extremely effective method for separating the luminescence signals from quartz and feldspars. Furthermore, D_e values obtained after infra-red stimulation and thermoluminescence generally agree within errors. This quantitative equivalence of those two sets of D_e values implies that as in the case of IRSL, TL signal is also feldspar-dominated. IRSL ages vary between 3.5 and 7.8 ka with associated errors up to 9%. Application of 'double SAR' protocol to coarse silt, closely-spaced deep-sea sediment samples seems advisable, despite the fact that the post-IR blue OSL signal is the most stable signal, and is preferred for dating.

KEYWORDS: Deep-Sea sediments; luminescence; dating; Mediterranean Sea; Hellenic Trench; 'double SAR'; IRSL

1. INTRODUCTION

Optically stimulated luminescence (OSL) dating of light-exposed sediments has rapidly developed over the past decade for terrestrial sedimentary applications and is increasingly used as a mean of establishing a sediment deposition chronology, in wide variety of late Quaternary studies. There has been considerable technological development in the last few years in the preferred mineral, instrumentation, and in various measurement protocols.

In particular, the recently developed single-aliquot regenerative-dose (SAR) procedure for quartz (Murray and Roberts, 1998; Murray and Wintle, 2000; 2003) enabled one estimation of the depositional age from each aliquot, reducing that way the amount of sample, measurement time, and sample preparation required. Since all the measurements are performed on one aliquot, normalization is not required. Regenerative-dose procedures have the additional advantage of using interpolation methods to determine the equivalent dose rather than extrapolation, as is required in additive-dose procedures (Blair et al., 2005). Therefore, SAR improves the precision of *De* estimates by just incorporating interpolative estimation techniques rather than extrapolative ones.

Despite the great development of luminescence dating procedures and the successful use of either thermoluminescence (TL), or OSL techniques in dating methodologies for terrestrial sedimentary applications, dating of marine environments and deep-sea sediments still remains a difficult task (Prescott and Robertson, 1997; Lian and Roberts, 2006). Deep-sea sediments were one of the first types of natural deposits investigated using luminescence dating (Wintle and Huntley, 1979; 1980). Only little further research has been undertaken in this area. For a summary of most deep-sea sediment dating studies employing both TL and OSL techniques in the following years (1980–2010), the reader could refer to Stokes et al. (2003a); Berger (2006) and Jacobs (2008).

Recently, the utilization of polymineral silt luminescence methods for dating deep-sea sediments was successfully assessed for the case of the uppermost 3 cm of muddy, seabed sediment collected from a deep-sea sediment core, drilled from a water depth of 4 km, near the deepest site of the Mediterranean Sea, outside Pylos, Greece (Polymeris et al., 2009). In the present study a new dataset is presented for the ages and sedimentation deposition rates for the same core using the feldspar-dominated infrared stimulated luminescence (IRSL) signals from polymineral silt-sized grains according to the 'double SAR' method of Banerjee et al. (2001). To the best of the author's knowledge and in contrast to numerous previous uses of the 'double SAR' method to Chinese Loess (Roberts and Wintle, 2001; Stokes et al., 2003b; Watanuki et al., 2003; Wang et al., 2006; Buylaert et al., 2007), the application of the specific procedure to deep-sea sediment dating was not previously reported. Therefore, the objective of the present study is to test for the first time its usefulness for closely-spaced deep-sea sediment samples by directly comparing the ages yielded both to the corresponding quartz-based optical as well as TL-based ages previously reported (Polymeris et al., 2009).

2. SAMPLING SITE AND PREPARATION

The Hellenic Trench system south of the Hellenic Arc, one of the world's most seismically active zones, is at present a zone of continental plate convergence, being one well defined boundary of the collision zone between the African-Arabian and European continental plates (Moores and Twiss, 1995). The Hellenic Arc-Trench system is part of the Alpine-Himalayan mountain system; this is one of the major structural features of the earth. Thus the Hellenic Arc-Trench system, one of the world's most tectonically active zones, provides a unique environment to study a variety of active sedimentological processes.

Although the sediments of the Mediterranean Sea are unique as regards luminescence dating, very little is known of the chronology of the neotectonic activity using luminescence dating techniques. Bottom sediment is mostly deposited from Aeolian transport directly into the site. There is a large contribution to this sediment originating from the nearby Sahara desert. Furthermore, the weather conditions in the ar-

ea, with periods of continuous and full sunshine could be beneficial to luminescence dating, increasing the possibility to zero the luminescence clock before deposition.

A 3 cm-long core of muddy, light brownish-gray calcareous sediment was collected from the operational site of the Neutrino Experimental Submarine Telescope with Oceanographic Research (NESTOR) experiment (Tzamarias, 2003), near the deepest site of the Mediterranean Sea. For a review on the geomorphologic characteristics of the site the reader could refer to Anassontzis et al., (1992); Trimonis and Rudenko (1992) and Polymeris et al. (2009). Location of sampling site is presented in Fig. 1.

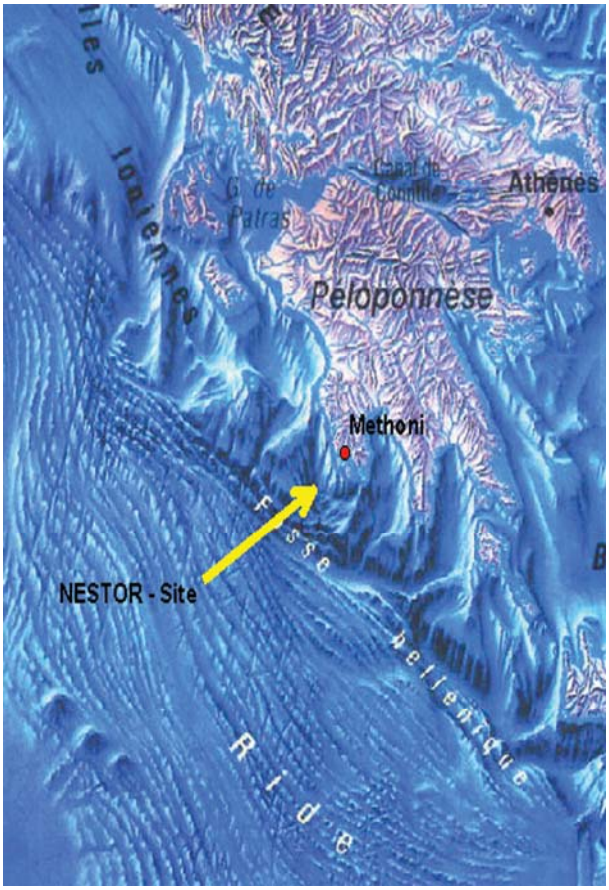

FIGURE 1: Map of the Southwest coast of the Peloponnesus in Greece. The arrow indicates the operational site of NESTOR, a broad plateau at a depth of about 4000 m. A little further away, one finds the deepest part of the Mediterranean Sea, at about 5200m.

A thin outer layer was removed in the laboratory and subsequently the core was divided in 3 to 4 mm thick layers-samples in subdued red filtered light conditions. Eventually, 7 samples were obtained. The density of the core was assumed to be uniform all over its volume, equal to 1.48 gr/cm^3 (Trimonis and Rudenko, 1992). Before treatment and etching, the dominant fraction grain size was found to be between 63 and 80 microns. The samples were sequentially treated, until the reaction ceased, with dilute hydrochloric acid (10% HCl) to remove carbonates, and with hydrogen peroxide (10% H_2O_2) to remove organic material (Aitken, 1985; Stokes et al., 2003). Next, the samples were treated with hydrofluoric acid (40% for 30 min) in order to remove surficial coatings. According to Rees-Jones (1995) and Stokes et al., (2003), in order to remove feldspars, the samples are treated with fluorosilicic acid. Therefore, while some mass of feldspathic material was certainly lost as a result of HF acid etching, all quartz grains were not eliminated since no treatment with fluorosilicic acid took place. Finally, polymineral coarse grains in the range 30-60 μm were extracted by wet sieving after etching. Grains of this dimension travel in air for an adequate time before deposition, so it is very probable that they are effectively bleached before sedimentation. Aliquots of the silt suspended in acetone were then precipitated onto 1 cm diameter aluminum discs (Aitken, 1985; Stokes et al., 2003).

The aforementioned characteristics of the samples (small core length, small sample thickness, continuous sampling in subsequent layers throughout the core's length), combined with the accumulation rate of the sediment (7-18 cm over 10 ka) and the large depth of the collection site, allow the possibility to investigate the accuracy and resolution for IRSL dating of closely-spaced deep-sea sediment samples in a deep sea site with extremely interesting features but without many previous luminescence records.

3. PROCEDURES AND PROTOCOLS

The IRSL signal from each sample disc was measured according to the single aliquot regenerative-dose (SAR) protocol, firstly introduced by Murray and Wintle (2000), after the modifications suggested by Banerjee et al., (2001) for polymineralic samples ('double SAR' method). According to Duller and Bøtter-Jensen (1993), after an IR exposure that bleaches the IRSL signal of a polymineral sample, a substantial OSL

signal is observed from feldspar grains. The 'double SAR' protocol procedure thus permits the determination of two equivalent dose (*De)* values for each aliquot; a polymineral IRSL *De* resulting mostly from feldspars and a polymineral post-IR OSL *De* for a mixed signal for quartz and feldspar grains (Duller, 1997). The experimental procedure is presented in Table 1.

Table 1. Optically stimulated luminescence double single-aliquot regenerative dose (double OSL-SAR) sequence (Banerjee et al., 2001).

1. Regenerative dose, D_i (i = 1 natural; i = 2, 3, 4, 5, 6 regenerative doses =4.25, 10.6, 18.7, 0 and 4.25 Gy)
2. Preheat (for 10 s)
3. Natural and regenerative dose IRSL for 100 s at 125°C (L_i)
4. Natural and regenerative dose blue OSL for 100 s at 125°C
5. Test dose, TD (=6.4 Gy)
6. Heat to 160 °C TL
7. Test dose IRSL for 100 s at 125°C (T_i)
8. Test dose blue OSL for 100 s at 125°C
9. Return to 1

The 'double SAR' method of Banerjee et al. (2001) stands as the first true SAR procedure dating application applied effectively to Chinese loess (Buylaert et al., 2008). It was invented and suggested since the extraction of fine-grained quartz from loess is at best a tedious operation, and in some cases it seems to be impractical, as in the case of Roberts and Wintle (2001); these authors were the first to apply this 'double-SAR' procedure to polymineral fine-grains of a Holocene sequence in the western site of the Chinese Loess Plateau. They found that the *De* values from the IR measurements were always greater than those derived from the (post-IR) blue OSL signals. The cause for the discrepancy was not resolved but the authors suggested that the (post-IR) blue OSL signal, dominated by quartz, yields the most reliable results. After a number of related studies attempting to isolate the luminescence signal arising form quartz by applying the 'double SAR' protocol to aliquots of mixed mineralogy (Thomas et al., 2003; Stokes et al., 2003; Watanuki et al., 2003; Wang et al., 2006), the quartz- dominated post-IR blue-light stimulated signal, measured with SAR, was found to yield the best results, although no independent age control was available to confirm the accuracy of the optical ages. The main disadvantage of the use of IRSL signals from polymineral fine-grains is that these signals are believed to come almost entirely from feldspar; a mineral which is known to suffer from anomalous fading (Spooner, 1994). This effect caused severe age underestimation. However, according to Buylaert et al., (2007), in the ~70 to ~130 ka age range, the 'double SAR' IRSL ages are, after allowance has been made for anomalous fading, in good agreement with the expected ages.

4. APPARATUS

All luminescence measurements were performed using the RISØ TL/OSL reader (model TL/OSL-DA-15), equipped with a high-power blue LED light source, an infrared solid state laser and a 0.085 Gy/s $^{90}Sr/^{90}Y$ β-ray source (Bøtter-Jensen et al., 2000). IRSL emission was measured at 125 °C, through a 7.5 mm Hoya U-340 filter. The power level was software controlled and set at 90% of the maximum power of the infrared solid state laser (875Δ10 nm), delivering at the sample position approximately 135 mW cm^{-2}. All signals are integrated over the first second of stimulation out of the 100 s of the entire curve. A background was subsequently subtracted based on the last 5 (95-100) s of stimulation. Although the choice of integration intervals for IRSL signal and background seems arbitrary, without any direct experimental validation, these were chosen in order to be identical with the respective integrals used for the grains of quartz, for direct comparison. Preheats and cut-heats were performed using a heating rate of 1°C/s.

5. IRSL CHARACTERISTICS

5.1 De versus preheat temperature

The influence of various preheat temperatures on the IRSL *De*, recuperation and recycling ratio values was investigated for the sample with laboratory code O1 using a fixed cut-heat at 160°C across the 130 to 260°C preheat temperature interval. Results are presented in the lower panel (A) of Fig.2 for the former,

whereas for both recuperation and recycling ratios in the lower panel (B) of the same Fig.

Equivalent doses almost form two plateaus, one for low preheat temperatures up to 160°C, and a second one for higher temperatures between 230 and 260°C. The high-temperature plateau value is substantially increased compared to the respective value of the low-temperature plateau. Furthermore, the agreement of the IRSL *De* values for each preheat temperature becomes worse as the latter increases. Finally, there is more scatter and larger errors associated with higher preheat temperatures, as the signals decrease.

For all the preheat temperatures applied, recycling ratio is close to unity, yielding relatively large errors. Finally, the increased recuperation values (≥ 8%) for all the preheat temperatures studied, stands as another worth mentioning feature of Fig. 2. Therefore, the preheat temperature of 160°C, already chosen as the preheat temperature for the rest of the measurements, provides trustworthy IRSL *De* values due to extremely low dispersion *De* value, a close to unity recycling-ratio-value and the lowest recuperation.

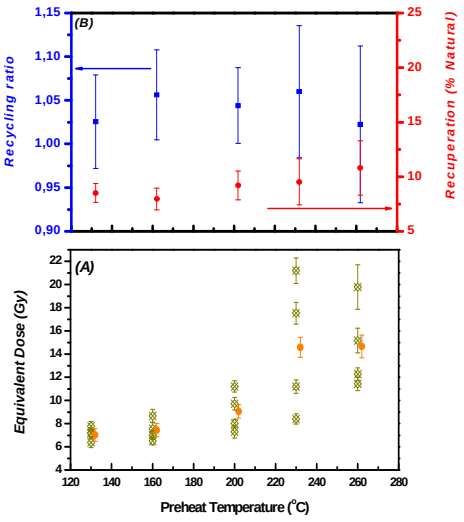

FIGURE 2: The dependence of equivalent dose (A), recuperation and recycling ratio values (B) on preheat temperature for samples collected from layer O1. Open symbols represent individually measured equivalent doses and filled symbols the mean values for each preheat temperature. Error bars indicate the 1σ deviation.

5.2 Dose Recovery test

The most stringent test regarding the applicability of any luminescence measuring protocol is a dose recovery test, namely whether the value of a previously delivered dose can be accurately and precisely determined.

Five fresh aliquots of each sample were put aside in order to perform a dose recovery test according to Murray and Wintle (2003). Two room temperature optical stimulations using the blue LEDs housed at the commercial RISØ TL/OSL systems for 100 seconds in order to bleach the aliquots, with 10-ks room temperature storage in between were used in an effort to mimic the natural conditions by first bleaching it without any heating procedure.

Dose recovery results are shown in Fig. 3. For all the aliquots, the ratio of the measured to given dose is within ±3% of unity, indicating the suitability of the IRSL signal from the 'double SAR' method to recover successfully the dose delivered to our samples.

This suitability, however, is not supported by either the large recuperation values, reaching the values of 8 – 11% of the initial natural signal, nor the increased recycling ratio, which lie well above unity, being in the range 1.05 – 1.08.

Nevertheless, the recuperation and recycling ratio criteria are known not to be particularly sensitive tests in order to affect the good dose recovery test (Murray and Wintle, 2003, Buylaert et al., 2008). An elevated temperature optical stimulation at the end of the natural dose cycle and each regenerative dose cycle, would possibly have reduced the recuperation observed on the IRSL signal, as Murray and Wintle (2003) reported that this helped in their quartz samples.

Of course, there is no a priori reason to think that the same experimental conditions should be equally suited to both quartz and feldspar grains on the same aliquot.

However, the direct comparison of the quartz and feldspar dose recovery test findings, presented already in the upper panel of Fig. 3, establishes experimentally that indeed this was the case for these samples.

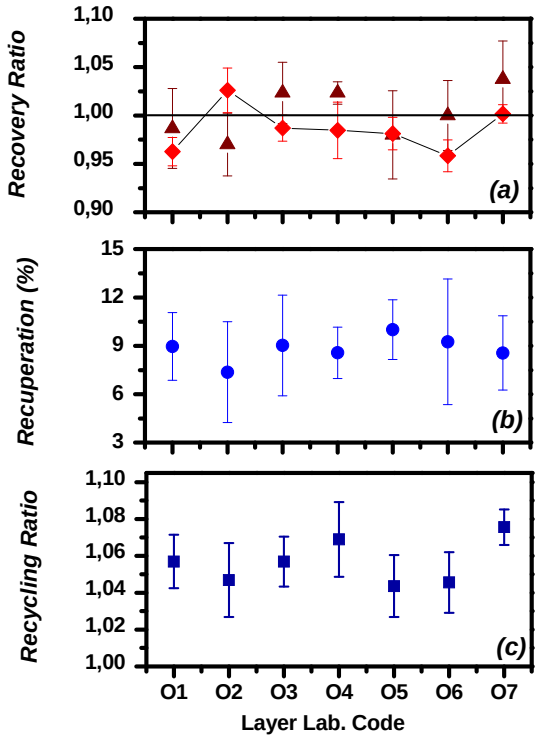

FIGURE 3: Data obtained from dose recovery experiments on 5 aliquots from each sample, using a 10s preheat at 160°C and a cut heat at 160°C, regarding the values of recycling ratio (a), recuperation (b), and recovery (measured to given dose) ratio (c). In the latter case, triangles represent recovery ratio for the IRSL signal while diamonds the corresponding post IR BSL values.

5.3 IRSL 'double SAR' results

Examples of typical IRSL decay curves for the natural signal (a), the three incremental regenerative doses, i.e. 4.25, 10.6 and 18.7 Gy (b, c and d respectively), the repeat dose point (e) and the recuperation afterwards (f), are presented in Fig. 4 for the first 40 s of stimulation. The inset of the same Fig. presents both IRSL and post-IR blue OSL decay curves for the natural signal in a logarithmic y scale. The presence of both intense luminescence signals is in great accordance with the quartzofeldspathic nature of the sample under study. Knowledge of the composition and original source of the mineral grains, in conjunction with the proportions and types of each siliciclastic mineral present within the polymineral silt aliquots would have been extremely useful. Unfortunately the quantity of the collected sediment was inadequate to perform such analysis. Thus the IR stimulated luminescence signal is believed to result from feldspars.

The IRSL signal is more intense compared to the respective post IR BSL, in terms of absolute luminescence intensities, providing a strong indication for a feldspar dominated mineralogy. Although both signals are very easy to bleach, a slower decay form with low residual level after 100 s stimulation is monitored for IRSL decay curve. Nevertheless, the rapid decay form with a relatively high residual level of post IR blue OSL is typically associated with a signal from quartz (Roberts, 2007; Afouxenidis et al., 2007). Fig. 4 indicates also that the illumination times used in both cases are adequate to empty traps responsible for both luminescence signals.

An illustrative diagram of a sensitivity-corrected growth curve for an aliquot of the sample O1 is plotted in Fig. 5. While the post IR blue OSL dose response curves showed slight curvature and thus were fitted for each aliquot mostly by a linear-plus-saturation-exponential growth function, the respective IRSL curves appear almost linear in the entire regeneration dose range. Therefore, all sensitivity corrected growth curves were fitted with a single linear function. This difference in the dose response curvature and shape provides the first strong indication regarding the effective isolation of the luminescence signals from these two minerals.

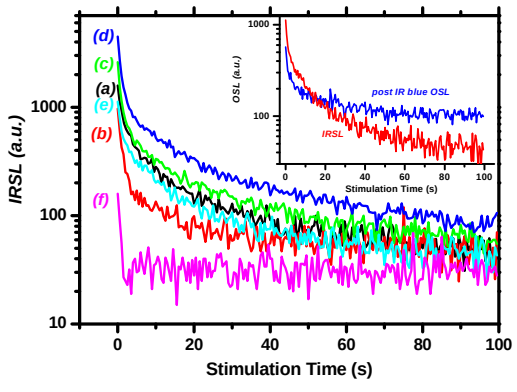

FIGURE 4: Typical IRSL decay curves for the natural signal (a), the three incremental regenerative doses, i.e. 4.25, 10.6 and 18.7 Gy (b, c and d respectively), the repeat dose point (e) and the recuperation afterwards (f), for the first 40 s of stimulation. Inset: IRSL and post IR OSL decay curves for the natural signal of the same aliquot, in a logarithmic y scale.

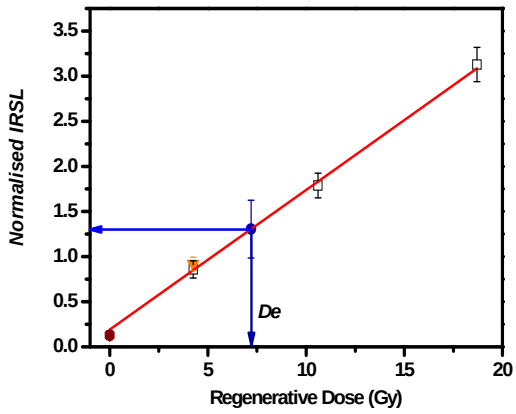

FIGURE 5: An IRSL growth curve, measured for an aliquot from the sample O1. *De* value is provided by interpolation of the natural IRSL signal (filled circle) onto the growth curve (line) resulting from the linear fit to the results of the measurement sequence (open squares). Filled triangle and hexagonal represent the recycle point and recuperation value respectively. Error bars indicate the 1σ deviation. The *De* value yielded is 7.4 Gy.

The IRSL equivalent doses obtained by applying the 'double SAR' protocol are plotted as circle symbols in radial manner in Fig. 6 for all layers (O1→O7).

The number of the aliquots measured is smaller for the first 2 samples, since a portion of these was consumed to perform the various tests.

The equivalent doses obtained for all layers show good reproducibility, despite the relative low number of aliquots measured. Furthermore, for each layer there seems to be a distribution of equivalent doses, shown as filled circle symbols.

Open circles represent measured values of *De,* which lie outside of the 2-σ region of each distribution.

For comparison sake, post IR blue OSL equivalent doses for all layers are also plotted in the same panels, represented as filled or open triangle symbols on the basis of whether they lie inside or outside respectively of the 2-σ region of the corresponding distribution.

However, a disadvantage of the method is reflected in the large relative errors of each IRSL *De* value, being of the order of 15-20%, without any pattern of change with depth.

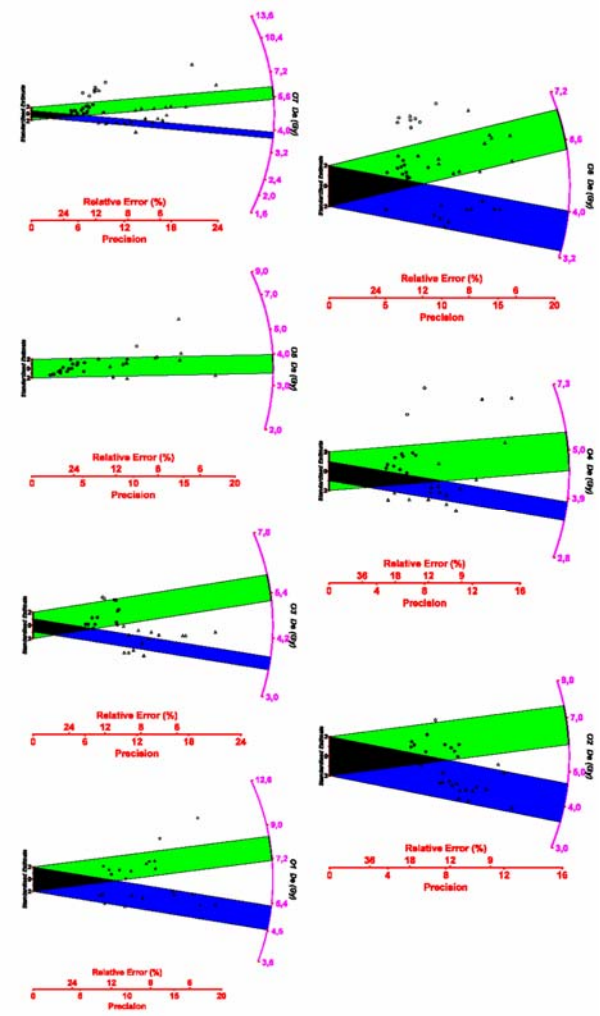

FIGURE 6: Radial plots for the equivalent doses measured for all samples (O1→O7). Each data point corresponds to an individual, single–aliquot equivalent dose estimation. The measured *De* (in Gy) for each aliquot can be read by tracing a line from the y-axis origin through the point, until the line intersects the radial axis on the right-hand. Corresponding standard error for each estimate can be read by extending a line vertically to intersect the x-axis. The latter has two scales: one plots the relative standard estimation of each *De* value (in %), while the other plots the reciprocal standard error, also termed as precision. Values with smallest relative errors and highest precisions are plotted closest to the radial axis. For each aliquot, two equivalent dose values were determined, derived from the IRSL and [post-IR] OSL signals. Therefore, for each layer both IRSL (circles) and post IR OSL (triangles) data points are presented in the same figure for the sake of comparison. Data points lying in the 2σ (green and blue bands respectively) regions are shown as filled points, otherwise as open.

Analysis of the data shows very good recycling ratio values. Although for all aliquots of all layers the latter is larger than 1, all values are

within 8% of unity. However, large recuperation values, of the order of 9-12.5% of the initial natural signal, indicate significant charge transfer due to preheating. There is no systematic behavior for the recycling ratios or the recuperation neither with depth nor with the equivalent doses yielded. Fig. 7 presents an example of IRSL and post IR blue OSL recuperation values (a) and recycling ratios (b) for each measured aliquot for the sample layer O5. The latter is considered as being typical and indicative at the same time, due to the fact that post IR blue OSL recuperation values for layer O5 are increased compared to all other layers, due to volcanic origin of the layer's material.

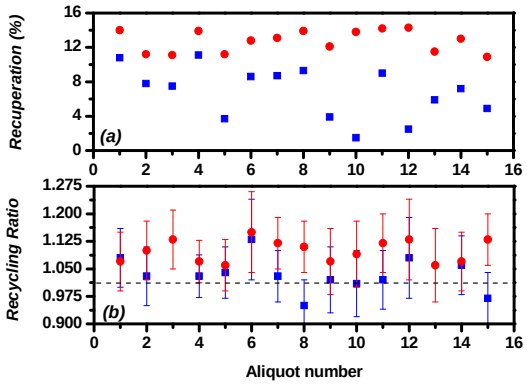

FIGURE 7: Typical examples of IRSL (circles) and post IR BSL (squares) recuperation values (a) and recycling ratios (b) for each measured aliquot for the sample layer O5.

Table 2: Summary of mean values of the luminescence D_e data.

Layer Lab. Code	Depth (mm)	TL D_e (Gy)	σ_{TL} (%)	IRSL D_e (Gy)	σ_{IRSL} (%)	#n_{IRSL}	*IRSL* RR	*IRSL* REC (%)	Post IR OSL D_e (Gy)	σ_{OSL} (%)	#n_{OSL}	Post IR OSL RR	Post IR OSL REC (%)	K_2O (%)	DR_{cor} (mGy/yr)
O1	29	9.78 ±1.18	12.1	7.74 ±0.47	6.1	11/11	1.07 ±0.06	11.6 ±4.6	4.80 ±0.13	2.8	11/11	1.03 ±0.06	3.6 ±2.8	1.61 ±0.09	1.04 ±0.03
O2	23.5	5.97 ±1.81	30.5	6.17 ±0.42	6.8	15/15	1.06 ±0.06	8.9 ±3.1	3.97 ±0.11	2.8	15/15	0.99 ±0.05	3.8 ±1.9	1.68 ±0.03	0.998 ±0.03
O3	19.5	5.65 ±0.71	12.5	5.57 ±0.44	7.9	15/15	1.05 ±0.07	9.7 ±4.4	3.82 ±0.08	2.0	15/15	1,02 ±0.07	4.5 ±2.4	1.70 ±0.01	1.01 ±0.03
O4	15.5	5.17 ±0.76	15.1	4.99 ±0.45	9.0	14/17	1.07 ±0.06	10.7 ±3.9	3.49 ±0.11	3.2	14/17	1.02 ±0.07	4.7 ±3.5	1.71 ±0.02	0.99 ±0.05
O5	12	$3.12 ±0.46	11.8	3.71 ±1.23	33.1	14/19	1.08 ±0.09	12.2 ±5.8	3.88 ±0.11	3	14/19	1.01 ±0.08	7.1 ±3.1	1.71 ±0.03	1.08 ±0.03
O6	8.3	6.27 ±0.65	10.5	5.87 ±0.43	7.3	13/22	1.06 ±0.05	9.9 ±3.9	3.53 ±0.10	2.8	11/22	0.98 ±0.07	3.9 ±2.5	1.77 ±0.03	1.08 ±0.04
O7	3.5	6.75 ±0.68	10.1	5.67 ±0.41	7.2	14/21	1.08 ±0.07	12.5 ±4.1	3.79 ±0.09	2.3	13/21	0.99 ±0.07	3.3 ±2.1	1.85 ±0.02	1.09 ±0.06

 # Number of aliquots used in the De estimation over the total number of aliquots measured

$ For layer O5, due to supralinearity correction: P = De + I = 3.12 + 0.79 = 3.91 (Gy)

A summary of the mean values of the IRSL D_e data throughout the core is presented in Table 2, along with the respective post IR blue OSL and TL results.

5.4 Anomalous fading

Given the problems frequently noted for anomalous fading (Wintle, 1973) of the feldspar signal, particularly of volcanic origin (Huntley and Lamothe, 2001), knowledge of whether the IRSL signal suffers from it becomes essential. For the anomalous fading tests, the approach of Liritzis et al. (2008) was adopted. One aliquot from every sample-layer was bleached by a SOL-2 solar simulator lamp (Dr. Hönle) and irradiated with 7 Gy of artificial beta dose. The aliquot was measured using IR and post-IR blue stimulation, irradiated with the same dose, preheated at 160°C for 10s and kept in a dark place for 90 days. Then the sample's IR and blue stimulated luminescence was measured again. Finally, a cycle of 3 irradiations with the same dose and readouts after IR and post-IR blue stimulation was performed to check the chang-

es on the sensitivity of each sample. The IR stimulations were performed for 100s at 125°C.

Results for the fading test experiment are presented in Table 3 only for the IRSL signal. As it becomes obvious, signal loss due to storage is of the order of 9 – 11% for all samples but O5, being almost 15%. However, sensitivity changes induced by repeated heating and dosing are comparable, being of the order of 5 – 8% per cycle. In other words, the net fading percentage is ~ 6% over three months for sample layer O5, but less than 4% for the other samples. For post IR OSL the signal loss is much less than the sensitivity change percentage which indicates absence of fading.

6. DOSIMETRY

Dose rates were determined from the concentrations of natural U, ^{232}Th and ^{40}K. These were determined by thick source alpha counting for ^{232}Th and natural U, and flame photometry for ^{40}K, in the form of K_2O. Dose rate calculations were made using the conversion factors of Adamiec and Aitken (1998). At 4 km of water depth, the dose rate resulting from cosmic rays is reduced by a factor of 10^6 (Prescott and Hutton, 1994). Only beta and gamma dose rates were considered in this work.

Dried and powdered sediment-sample from the outer layer of the core was analyzed using thick source alpha counting with a ZnS detector. The measurements were performed both in the integral and in the pair counting mode, for the discrimination between Th and U. Concentrations of ^{234}U are assumed to be in excess of ^{238}U, as expected for carbonaceous marine sediments (Ivanovich and Harmon, 1992; Wagner, 1998; Berger, 2006) and also in excess of the ^{230}Th concentrations. Unfortunately the quantity of the collected sediment was inadequate to perform individual measurements in each layer. It was assumed that natural U and ^{232}Th concentrations were uniformly distributed all over the sample. Moreover, the excess of ^{230}Th and ^{231}Pa content would impose time-dependent changes to the dose rate. However, due to the low independent age estimates of 3 ka from the area, based on Planktonic foraminiferal ages determined by AMS ^{14}C measurements (Trimonis and Rudenko, 1992), unsupported uranium isotopes would produce only a relatively small, <7-10% systematic upward shift in dose rates (Kokkoris and Liritzis, 1997). Therefore, we concluded that estimation of the excesses of daughter isotopes ^{210}Pb, ^{230}Th and ^{231}Pa was not required and the same U and ^{232}Th concentrations were used throughout the core. Two measurements with duration longer than 5 days each were carried out, according to the methodology proposed by Aitken (1985). The sample gave sealed over unsealed ratio of 1.174, which is considered as to represent significant Rn escape under laboratory conditions (Aitken, 1985). Thick source alpha counting resulted in concentrations of ~4±0.18 ppm in U and of ~6±0.6 ppm of ^{232}Th. For the determination of ^{40}K, flame photometry was used. Potassium concentration is expressed as K_2O % w/w per sample. Results are presented in Table 2.

The range of β particles is only a few mm, so the beta dose rate reaches its full value within 1 or 2 mm of the layer's surface. Natural γ rays travel many cm in sediment, reaching their full value within 30 cm of the surface for sediments with a density value of 2 g cm^{-3} (Aitken, 1985).

For the effect of burial depth on γ dose rate, the approach of Madsen et al. (2005) was adopted. The variation of the γ dose-rate contribution was taken from Aitken (1985), with correction for the average density of the core (1.48 g cm^{-3}). The curve was parameterized to give the equation:

$$D'_{\gamma,dry} = D'_{\gamma,dry,\inf}\left(0.5 + 0.11305\left(1 - e^{-\frac{x}{2.06096}}\right) + 0.38515\left(1 - e^{-\frac{x}{11.47976}}\right)\right)$$

Here x stands for the cores length form its top. Fitting parameters are slightly different from those obtained by Madsen et al. (2005). Integrating and averaging between the surface and a given depth one can find time averaged gamma dose rates, assuming a linear sedimentation rate:

$$D'_{\gamma,dry,av} = D'_{\gamma,dry,\inf}\left(0.9982 - \frac{0.233}{x}\left(1 - e^{-\frac{x}{2.06096}}\right) - \frac{4.42}{x}\left(1 - e^{-\frac{x}{11.47976}}\right)\right)$$

where $D'_{\gamma,dry,av}$ is the average gamma dose rate in dry sediment and $D'_{\gamma,dry,inf}$ is the infinite matrix gamma dose rate in dry sediment, at depth x (cm).

Water, as well as organic matter, acts as a radiation-absorber; they absorb some of the radiation energy and hence reduce the dose rate. Because of the high organic content of the core, the usual formulae need modification. Our treatment is that of Lian et al. (1995). A sample is considered to be composed of three components: mineral (m), organic (o) and water (w). Defining the organic to mineral (Δ^o) and water to mineral (Δ^w) ratios as $\Delta^o = m_o / m_m$ and $\Delta^w = m_w / m_m$ (m_i represents the mass of component i), dose rates are provided by the equations:

$$D'_{\beta} = \frac{D'_{\beta,dry}}{1 + 1.2 \cdot \Delta^o + 1.25 \cdot \Delta^w}$$

$$D'_{\gamma} = \frac{D'_{\gamma,dry,av}}{1 + 1.1 \cdot \Delta^o + 1.14 \cdot \Delta^w}$$

Dose rates and its uncertainties are presented for each layer in Table 2.

7. RESULTS AND DISCUSSION

7.1 IRSL versus OSL and TL values of De

As it becomes obvious from both Table 2 and Fig. 6, the *De* values yielded from the IRSL measurements are, with one exception, always greater than for the (post-IR) blue OSL signal. This result stands in great agreement with the findings of Roberts and Wintle (2001) to polymineral fine-grains of a Holocene sequence in the western site of the Chinese Loess Plateau. After the most of the feldspar signal has been previously stimulated by IR radiation, the blue stimulated post-IR blue OSL is quartz dominated signal. Feldspar dominated mineralogy within polymineral silt aliquots of the present study might offer a possible explanation for this systematic difference.

Furthermore, as Table 2 goes on to reveal, mean D_e values obtained after infra-red stimulation and TL generally agree within errors; in fact they coincide for layers (O2→O6). This conclusion is also strongly supported by Fig. 8, where all luminescence equivalent doses are plotted as a function of depth. Both TL (square symbols) and corresponding IRSL (circle symbols) values of *De*, show the exact same pattern of down core variation, increasing with depth, below the first centimetre where, within errors, these values are indistinguishable.

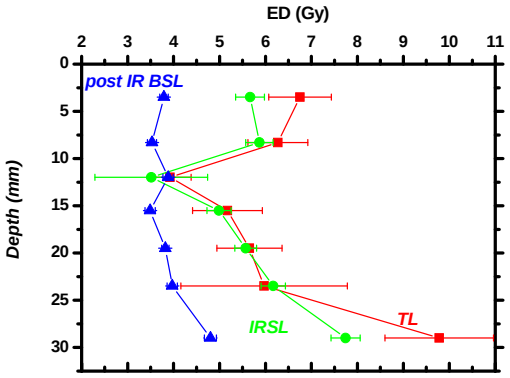

FIGURE 8: Down core variation of equivalent doses measured using IRSL (filled circles), TL (filled squares) and post IR OSL (filled triangles). Error bars are ±1σ deviation. Average OSL De values do not include the outliers.

This quantitative equivalence of those two sets of D_e values implies that as in the case of IRSL, TL signal is also feldspar-dominated, despite the fact that it arises from both quartz as well as feldspars. However, in a situation where the ratio of feldspar to quartz is very high, either by mass or intensity, one expects the post IR blue OSL signal to be also dominated by feldspar. That was exactly the case of Roberts (2007); applying the double SAR protocol to untreated polymineral material from a sample of loess from Bignell Hill, Nebraska to both fine grains and coarse silt, she did not enable isolation of a signal dominated by quartz. Instead, both IRSL and post IR BSL signals appeared to be dominated by the signal from feldspars. For-

tunately, according to the preceding, this is not the case of the present study.

One notable exception among all layers is presented for sample layer O5, where all three stimulation modes (IRSL, post IR blue OSL and TL) provide, within errors, similar equivalent doses. However, in the case of IRSL, this value is somehow lower compared to the other two. This discrepancy could be possibly attributed to the geochemical composition of sample O5, which was previously determined using X Ray Diffraction (XRD) spectroscopy (Polymeris et al., 2009). According to these results, sample O5 consists primarily of tephra resulting from the eruption of Santorini's volcano while feldspars were hardly detected. This conclusion was further supported by both its luminescence properties, and the luminescence ages. However, major geochemical analysis undertaken for the sample O5 did not reveal the presence of any feldspar. Thus the IR stimulated luminescence signal is not resulting from feldspars, but from other volcaniclastic minerals such as Al_2O_3 and mica. The latter is known to give rise to an IRSL signal (Clark and Sanderson, 1994). The absence of feldspar in the minerals of O5 sample could also provide an explanation regarding the large (33%) relative uncertainty on the IRSL mean D_e value. Finally, the presence of such materials of volcanic origin in the deposits of sample O5 is clearly a concern given the problem of anomalous fading, which resulted in the lower IRSL equivalent dose yielded for the sample.

7.2 IRSL ages

Feldspars have an internal ^{40}K radiation source (Aitken, 1985), which needs to be taken into account when determining the dose rate. For a typical potassium-rich grain, this would increase the dose rate by up to about 30% (Vafiadou et al., 2007), while in the case of a sodium-rich grain this contribution was calculated at about 17% (Walinga et al., 2002). However, a mixture of different kinds of feldspars is more likely to be present rather than a single one type of feldspar. Unfortunately the composition of each layer-sample was not determined because the quantity of the collected sediment was inadequate to perform such analysis. Therefore, the internal ^{40}K radiation source was not taken into account. IRSL and TL ages are, with one exception, ~1.5 times larger than those from the post IR blue OSL approach. However, in the case of potassium-rich grains, an increase of the dose rate by up to about 30%, as suggested by Vafiadou et al. (2007) would have resulted in comparable results with quartz-based optical dating results. IRSL ages, with associated errors up to 9%, are listed in Table 2 along with the respective post IR blue OSL and TL results. Quartz-based optical dating was proved to be relatively successful, due to consistency with AMS ^{14}C radiocarbon ages obtained from Planktonic foraminifera.

Especially in the case of feldspar dominated mineralogy within polymineral silt aliquots of the present study, the used total dose rates in the case of both IRSL as well as TL measurements are inaccurate, since a significant fraction of the dose rate arises from K. Assuming a mix of potassium and sodium rich feldspars, it is feasible to assume that the dose rates in the case of both IRSL and TL ages are increased by 20%. However, it is unlikely that the magnitude of this effect would generate a change in the dose rate of ~1.5 factor, as required here to reconcile the TL and IRSL with the respective OSL ages. It will just place the TL ages closer to the OSL ages.

Alternatively, this discrepancy could be attributed to the different bleaching rate of post IR blue OSL signal of quartz compared to the thermoluminescence and IRSL signals which mostly result from feldspars. This is also strongly supported by the inset of Fig. 4, where the post IR OSL signal reaches its residual level much faster compared to the respective IRSL decay curve. Finally, three additional explanations could be provided by the arguments of Roberts and Wintle (2001), i.e (a) incomplete bleaching of the IRSL signal prior to deposition, (b) charge transfer and (c) initial sensitivity changes. Among those three the two former stand as the most prominent, due to underwater bleaching experienced by the grains during deposition. The latter is less effective, because grains are not exposed to direct sunlight, but experience a more restricted spectrum due to

absorption and scattering in the water column, especially due to the large depth of the site.

7.3 The Santorini eruption

According to table 3, the layer O5 yields the youngest luminescence age, presented in the study independent on the stimulation mode, ranging between 3.25 - 3.6 ka. This age estimate corresponds to the time of the eruption of the Santorini (Thera) volcano. This eruption has already attracted a great scientific interest, dated to 1624 B.C. from tree-rings, 1645±20 B.C. from ice-cores and between 1400 and 1700 B.C. by radiocarbon measurements (Hardy and Renfrew, 1990; Friedrich et al., 2006; Liritzis et al, 1996). This similarity between luminescence ages from all three signals strongly supports the argument towards volcanic origin of the sample O5 from the Santorini eruption.

Table 3: Summary of luminescence ages along with IRSL fading results.

Layer Lab. Code	Depth (mm)	IRSL age (ka)	σIRSL age (%)	OSL age (ka)	σOSL age (%)	TL age (ka)	σTL age (%)	IRSL fading (sensitization) (%)
O1	29	7.45 ±0.55	7.2	4.61 ±0.28	6.0	9.40 ±1.52	16.2	9.1 (5.3)
O2	23.5	6.18 ±0.42	7.1	3.97 ±0.24	6.1	5.98 ±1.93	33.5	10.2 (5.9)
O3	19.5	5.51 ±0.39	7.3	3.78 ±0.21	5.5	5.59 ±1.01	17.9	9.8 (4.9)
O4	15.5	5.04 ±0.39	7.2	3.51 ±0.23	6.7	5.18 ±0.87	16.8	11 (6.3)
O5	12	3.25 ±1.33	41.3	3.61 ±0.22	6.1	3.62 ±0.57	15.6	15 (8.9)
O6	8.3	5.43 ±0.47	8.7	3.27 ±0.21	6.4	5.81 ±0.78	13.6	10.3 (5.8)
O7	3.5	5.20 ±0.51	9.1	3.47 ±0.26	7.4	6.20 ±0.92	14.8	9.4 (6.1)

Equivalent dose values yielded for all three luminescence techniques are, within errors, in excellent agreement, implying a prolonging heating in the past. The impact of that heating was so strong in order for all the related traps to be totally emptied, so that the three independent stimulation modes could suggest the same equivalent dose value, consequently the same age as well.

Here it is suggested that the sample O5 consists of material that was heated during the Santorini volcanic eruption. The eruption is the only known physical phenomenon which involves a procedure of prolonged heating in the appropriate time interval.

The presence of sharp TL peaks in the sample, especially the one at 110^{o}C rather than one broad TL emission suggests the presence of quartz rather than glass (Berger and Huntley, 1983).

Another luminescence features suggesting the presence of quartz are both the supralinearity indicated in the case of β regenerated TL growth curve along with the relative large recuperation value for layer O5 (Tsukamoto et al., 2003).

The tephra from the Santorini volcano is known to contain quartz (Hardy and Renfrew, 1990; Liritzis & Galloway 1996; Friedrich et al., 2006). For a thorough geochemical analysis report regarding the sample O5, readers could refer to Polymeris et al (2009).

8. CONCLUSIONS

In the present study, a new, 'double SAR' IRSL dataset is presented for the sedimentation ages of a deep-sea sediment core of the Hellenic Trench, drilled from a water depth of 4 km, near the deepest site of the Mediterranean Sea, outside Pylos, Greece.

IRSL results seem very much alike with the respective TL results, indicating thus the feldspar dominated mineralogy of the samples under study.

However, the lack of quantitative equivalence between the IRSL and post IR blue OSL sets of D_e values provides a strong argument towards the use of the 'double SAR' protocol for effective separating the luminescence signals resulting from quartz and feldspars.

Finally, the results of the present study fully support the conclusion of both Banerjee et al. (2001) and Roberts and Wintle (2001) that the (post-IR) OSL signal is the most stable signal, and is preferred for dating.

REFERENCES

Adamiec, G, Aitken, M.T (1998) Dose – rate conversion factors: update, *Ancient TL* 16, 37 – 49.

Afouxenidis, D, Stefanaki, E.C, Polymeris, G.S, Sakalis, A, Tsirliganis, N.C, Kitis, G (2007) TL/OSL properties of natural schist for archaeological dating and retrospective dosimetry, *Nuclear Instruments and Methods In Physics Research A* 580, 705 – 709.

Aitken, M.J (1985) *Thermoluminescence Dating*. Academic Press, London

Anassontzis, E, et al (NESTOR Collaboration) (1992) NESTOR: A neutrino particle astrophysics underwater laboratory for the Mediterranean. *Proceedings from the « 2nd NESTOR International Workshop »*, pp 1.

Banerjee, D, Murray A.S, Bøtter – Jensen, L, Lang, A (2001) Equivalent dose estimation using a single aliquot of polymineral fine grains, *Radiation Measurements* 33, 73 – 94.

Berger, G.W (2006) Trans-arctic-ocean tests of fine-silt luminescence sediment dating provide a basis for an additional geochronometer for this region, *Quaternary Science Reviews* 25, 2529 – 2551.

Blair, M.W, Yukihara, E.G, McKeever S.W.S (2005) Experiences with single-aliquot OSL procedures using coarse-grain feldspars, *Radiation Measurements* 39, 361 – 374.

Bøtter – Jensen, L, Bulur, E, Duller, G.A.T, Murray, A.S (2000) Advances in luminescence instrument systems, *Radiation Measurements* 32, 523 – 528.

Buylaert, J.P, Vandenberghe, D, Murray A.S, Huot, S, De Corte, F, Van den Haute, P (2007) Luminescence dating of old (>70 ka) Chinese loess: A comparison of single-aliquot OSL and IRSL techniques *Quaternary Geochronology* 2, 9 – 14.

Buylaert, J.P, Murray, A.S, Vandenberghe, D, Vriend, M, De Corte, F, Van den Haute, P (2008) Optical dating of Chinese loess using sand-sized quartz: Establishing a time frame for Late Pleistocene climate changes in the western part of the Chinese Loess Plateau, *Quaternary Geochronology* 3, 99 – 113.

Clark, R.J, Sanderson, D.C.W (1994) Photostimulated luminescence excitation spectroscopy of feldspars and micas, *Radiation Measurements* 23, 641–646.

Duller, G.A.T (1997) Behavioural studies of stimulated luminescence from feldspars, *Radiation Measurements* 27, 663–694.

Duller, G.A.T, Bøtter – Jensen, L (1993) Luminescence from potassium feldspars stimulated by infrared and green light, *Radiation Protection Dosimetry* 47, 683 - 688.

Friedrich, W.L, Kromer, B, Friedrich, M, Heinemeir, J, Pfeiffer, T and Talamo, S (2006) Santorini Eruption Radiocarbon Dated to 1627–1600 B.C., *Science*, 28, 2006, 548, plus online supplemental material

Huntley, D.J, Lamothe, M (2001) Ubiquity of anomalous fading in K-feldspars, and the measurement and correction for it in optical dating, *Canadian Journal of Earth Sciences* 38, 1093–1106.

Jacobs, Z (2008) Luminescence chronologies for coastal and marine sediments, *Boreas* 37, 508 – 535.

Knoll, F.G (1999) *Radiation Detection and Measurements*. 3rd Edition, J. Whiley & Sons, Inc.

Kokkoris, M and Liritzis, Y (1997) Dose versus time for U-Disequilibrium and revised dose-rate data for TL/ESR dating, *European journal of PACT*, No. 45. IV. 5, 281 – 294

Lian, O.B, Roberts, R.G (2006) Dating the Quaternary: progress in luminescence dating of sediments, *Quaternary Science Reviews* 25, 2449 – 2468.

Liritzis, I, Kitis, G, Galloway, R.B, Vafiadou, A, Tsirliganis, N.C, Polymeris, G.S (2008) Probing luminescence dating of archaeologically significant carved rock types, *Mediterranean Archaeology and Archaeometry*, Vol. 8, No. 1, pp. 61-79.

Liritzis I., Michael C. and Galloway R.B. A (1996) A significant Aegean volcanic eruption during the second millennium B.C. revealed by thermoluminescence dating. *Geoarchaeology Internat.*, 11, 4, 361-371.

Moores, E.M, Twiss, R.J (1995) *Tectonics*. W. H. Freeman, New York.

Murray, A.S, Roberts, R.G (1998) Measurement of the equivalent dose in quartz using a regenerative-dose single-aliquot protocol, *Radiation Measurements* 29, 503 - 515.

Murray, A.S, Wintle, A.G (2000) Luminescence dating of quartz using an improved single – aliquot regenerative – dose protocol, *Radiation Measurements* 32, 57 – 73.

Murray, A.S, Wintle, A.G (2003) The single aliquot regenerative dose protocol: potentials for improvements in reliability, *Radiation Measurements* 37, 377 – 381.

Polymeris, G.S, Kitis, G, Liolios, A.K, Tsirliganis, N.C, Zioutas, K (2006) Minerals as Time – Integrating Luminescence Detectors for setting bounds on Dark Matter Particle Characteristics, *Nuclear Instruments and Methods In Physics Research A* 562, 207 – 213.

Polymeris, G.S, Kitis, G, Liolios, A.K, Sakalis, A, Zioutas, K, Anassontzis, E.G, Tsirliganis, N.C (2009) Luminescence dating of the top of a deep water core from the NESTOR site near the Hellenic Trench, east Mediterranean Sea, *Quaternary Geochronology* 4, 68 – 81.

Prescott, J.R, Hutton, J.T (1994) Cosmic ray contributions to dose rates for luminescence and ESR dating: large depths and long-term time variations, *Radiation Measurements* 23, 497 – 500.

Prescott, J.R, Robertson, G.B (1997) Sediment dating by luminescence; a review, *Radiation Measurements* 27, 893 – 922.

Roberts, H.M (2007) Assessing the effectiveness of the double-SAR protocol in isolating a luminescence signal dominated by quartz, *Radiation Measurements* 42, 1627 – 1636.

Roberts, H.M, Wintle, A.G (2001) Equivalent dose determinations for polymineralic fine-grains using the SAR protocol: application to a Holocene sequence of the Chinese Loess Plateau, *Quaternary Science Reviews* 20, 859 – 863.

Roberts, H.M, Wintle, A.G (2003) Luminescence sensitivity changes of polymineral fine grains during IRSL and [post – IRSL] OSL measurements, *Radiation Measurements* 37, 661 – 667.

Spooner, N.A (1994) The anomalous fading of infrared stimulated luminescence from feldspars, *Radiation Measurements* 23, 625–632.

Stokes, S, Hetzel, R, Bailey, R.M, Mingxin, T (2003b) Combined IRSL–OSL single-aliquot regeneration (SAR) equivalent dose (De) estimates from source proximal Chinese loess, *Quaternary Science Reviews* 22, 975 – 983.

Stokes, S, Ingram, S, Aitken, M.J, Sirocko, F, Anderson, R, Leuschner, D (2003a) Alternative chronologies for late quaternary (Last Inerglacial – Holocene) deep sea sediment via optical dating of silt – size quartz, *Quaternary Science Reviews* 22, 925 – 941.

Thomas, P.J, Murray, A.S, Sandgren, P (2003) Age limit and age underestimation using different OSL signals from lacustrine quartz and polymineral fine grains, *Quaternary Science Reviews* 22, 1139 – 1143.

Trimonis, E, Rudenko, M (1992) Geomorphology and bottom sediments of the Pylos area. *Proceedings from the « 2nd NESTOR International Workshop »*, pp 321.

Tzamarias, S.E (2003) NESTOR: a deep-sea neutrino telescope, *Nuclear Instruments and Methods In Physics Research A* 502, 150 – 154.

Vafiadou, A, Murray, A.S, Liritzis, I (2007) Optically stimulated luminescence (OSL) dating investigations of rock and underlying soil from three case studies, *Journal of Archaeological Science* 34, 1659 – 1669.

Wallinga, J, Murray, A.S, Bøtter – Jensen, L (2002) Measurement of the dose in quartz in the presence of feldspar contamination, *Radiation Protection Dosimetry* 101, 367 – 370.

Wang, X, Lu, Y, Zhao, H (2006) On the performances of the single-aliquot regenerative-dose (SAR) protocol for Chinese loess: fine quartz and polymineral grains, *Radiation Measurements* 41, 1–8.

Watanuki, T, Murray, A.S, Tsukamoto, S (2003) A comparison of OSL ages derived from silt-sized quartz and polymineral grains from Chinese loess, *Quaternary Science Reviews* 22, 991–997.

Wintle, A.G, Huntley, D.J (1979) Thermoluminescence dating of a deep-sea ocean core, *Nature* 279, 710-712.

Wintle, A.G, Huntley, D.J (1980) Thermoluminescence dating of ocean sediments, *Canadian Journal of Earth Sciences* 17, 348–360.

Wintle, A.G (1973) Anomalous fading of thermoluminescence in mineral samples, *Nature* 245, 143–144.